Spacecraft Trajectory Design Strategies Based on Close Encounters with a Smaller Primary in a 4-body Model

Kathleen C. Howell[1] and Diane Craig Davis[2]
Purdue University, West Lafayette, Indiana, 47905

In spacecraft trajectory design, ΔV is limited and it becomes necessary to alter the characteristics of an orbit through other means. For example, close encounters of one or several moons in a planetary system can be employed to alter the shape of the orbit. Also, if the spacecraft is oriented favorably with respect to the sun, the solar gravity can be employed to alter the shape of the planetary orbit. When combined, the results can be dramatic. In this investigation, an efficient strategy to incorporate multiple gravity fields in the initial trajectory design process is explored.

I. Introduction

Traditionally, patched-conic analysis has dominated preliminary design approaches for interplanetary missions that are comprised of multiple flybys and include satellite tours such as Galileo,[1] Cassini,[2-4] and a proposed Europa Orbiter mission.[5-7] However, incorporating multiple gravity fields in the dynamical model, early in the tour design process, could expand the design options for future missions. The simplest element in such a strategy is a flyby and, thus, an examination of flybys from a multi-body perspective is insightful. Of course, gravity assists have been investigated and exploited very successfully for decades. Nevertheless, incorporating the gravity of the encounter body explicitly during the early design process more accurately reflects the flyby characteristics and might add trajectory options. This is particularly important in certain regimes where the gravity fields of multiple bodies impact the spacecraft behavior to a similar degree and must be simultaneously considered. For example, in the tour design of a proposed Europa Orbiter mission in 1997, Sweetser et al. note that conic analysis is inappropriate for the study of ballistic capture at Europa, yet a good set of initial conditions is essential in such a nonlinear problem.[7] Examination of the problem of incorporating multiple gravitational bodies in trajectory design is ongoing by many researchers. For example, Ross et al. employed a method based on patching three-body arcs in the design of a tour proposed for the Jupiter system with a final arrival into an orbit about Europa without an insertion maneuver.[8] Howell and Guzmán[9] incorporated flybys in an accurate multi-body model; while successful, its high level of accuracy and semi-analytical formulation is too complex in an initial design process to seek a quick and efficient strategy. An energy kick function is an alternative intermediate step between a patched-conic approximation and an integrated multi-body propagation. While the effect of the flyby is modeled with the kick function as a discrete event occurring at the spacecraft's closest approach to the flyby body, the expression for the energy kick function is derived from the Jacobi Constant in the three-body problem rather than the analytical relationships from the conic solution. The kick function parameterizes the change in orbital energy via the periapse angle, ω_r, relative to the planet-moon rotating x-axis.

Various investigations of orbits in multi-body regimes, including comets and other solar system particles, as well as spacecraft, employ the kick function to lend insight to the problem. Malyshkin and Tremaine[10] represent the kick function as a continuous interpolation function determined from a numerically integrated set of trajectories and apply it to the problem of the orbital evolution of comet trajectories, considering the probabilities of cometary survival. Zhou, Sun, Zheng, and Valtonen[11] derive the kick function from an expansion of the equations of motion in the Circular Restricted 3-body Problem (CR3BP) and employ it to study the transfer of comets from the Oort cloud to the inner solar system due to the gravitational effects of Jupiter. Pan and Sari[12] integrate the torque exerted

[1] Hsu Lo Professor of Aeronautical and Astronautical Engineering, School of Aeronautics and Astronautics, Purdue University, Armstrong Hall, 701 W. Stadium Ave., West Lafayette, Indiana 47907-2045; Fellow AAS; Associate Fellow AIAA.
[2] Ph.D. Student, School of Aeronautics and Astronautics, Purdue University, Armstrong Hall, 701 W. Stadium Ave., West Lafayette, Indiana 47907-2045.

on a particle by the gravity of a perturbing body. Then, their resulting kick function is the basis for an investigation of the motion of particles originally in nearly circular orbits around a star (with Jacobi Constant ≥ 3) that encounter a planet and are perturbed into highly eccentric orbits. Ross and Scheeres[13] generate the kick function using Picard's method of successive approximations and apply it to distant flybys of a perturbing moon; a spacecraft remains outside of the Hill sphere in the planet-moon system and the periapsis of the spacecraft orbit remains beyond the moon's orbital radius.

In this work, the impact of a close flyby on specific spacecraft mission design scenarios is considered. The energy kick function is presented and applied in the Saturn-Titan system, specifically for orbits that dip below the radius of Titan. For a given set of initial conditions at the spacecraft orbit apoapsis, the kick function is employed to set up a Titan flyby that modifies the semi-major axis, a, of the orbit by a pre-determined amount. To achieve a specific increase or decrease in semi-major axis, that is, Δa, the appropriate angle of periapsis with respect to the rotating x-axis, ω_r, is targeted by adding a small ΔV to the initial state. The kick function is employed to estimate the required target angle ω_r. Because of the assumptions and approximations involved in the derivation of the kick function, this estimate is not sufficiently accurate to achieve the desired change in semi-major axis precisely for arbitrary initial conditions. Therefore, the estimate is improved by adding an appropriate offset to the target angle. Finally, a solar gravity perturbation is added to the analysis, and its effect on the numerical integration is investigated. The goal of this work is to use the kick function to target an appropriate periapsis angle to achieve a desired change in semi-major axis for eventual application to multiple flybys in trajectory design.

II. Background

To describe the effects of a flyby on a spacecraft orbit, the equations of motion are written in terms of the CR3BP. A fourth-body perturbation is included in the equations to model, for example, the sun's gravity on a spacecraft in a planet-moon system. The integral of the motion in the CR3BP, the Jacobi Constant, is employed to derive an energy kick function that characterizes the change in the spacecraft orbit due to a close encounter with the smaller primary.

A. Dynamical model

The equations of motion for a vehicle moving under the influence of multiple gravity fields can be formulated in terms of various coordinates and reference frames. Most familiar, perhaps is the motion in an inertial reference frame where the position of the spacecraft relative to an inertially fixed point is expressed in terms of a set of inertial coordinates X, Y, and Z. Then, the equations of motion of a spacecraft, under the influence of N gravity fields, are written

$$\begin{aligned}
\ddot{X} &= \frac{-GM_1X_1}{r_1^3} - \frac{GM_2X_2}{r_2^3} - \cdots - \frac{GM_NX_N}{r_N^3} \\
\ddot{Y} &= \frac{-GM_1Y_1}{r_1^3} - \frac{GM_2Y_2}{r_2^3} - \cdots - \frac{GM_NY_N}{r_N^3} \\
\ddot{Z} &= \frac{-GM_1Z_1}{r_1^3} - \frac{GM_2Z_2}{r_2^3} - \cdots - \frac{GM_NZ_N}{r_N^3}
\end{aligned} \tag{1}$$

where $\bar{r}_i$ is the position vector from gravitational body P_i to the spacecraft and r_i is the magnitude of the position vector. (Note that vectors are indicated with an overbar.) For the problem of three or four bodies, a rotating reference frame along with certain assumptions can provide insight to the problem. Initially, let there be three bodies in the system.

The motion of a spacecraft moving under the gravitational influences of two larger bodies, such as a planet and a moon, can be described in terms of the CR3BP. In this model, the two primaries, P_1 and P_2, are assumed to be orbiting their barycenter on circular paths, while the spacecraft is assumed to possess negligible mass. A set of rotating axes appears in Fig. 1 and moves with the P_1-P_2 system. The x-axis is directed from P_1 to P_2, the z-axis is normal to the plane of motion of the two primaries and parallel to the primary orbital angular momentum, and the y-axis completes the right-handed system. Representing the distance between the spacecraft and the two primaries as r_1 and r_2, the equations of motion for the spacecraft are

$$\ddot{x} - 2n\dot{y} - xn^2 = -\frac{(1-\mu)(x+\mu)}{r_1^3} - \frac{\mu(x-(1-\mu))}{r_2^3}$$
$$\ddot{y} + 2n\dot{x} - yn^2 = -\frac{(1-\mu)y}{r_1^3} - \frac{\mu y}{r_2^3} \tag{2}$$
$$\ddot{z} = -\frac{(1-\mu)z}{r_1^3} - \frac{\mu z}{r_2^3}$$

where x, y, and z are the position coordinates of the spacecraft in terms of the rotating frame, n is the mean motion of the P_1-P_2 system, and μ is the nondimensional gravitational parameter,

$$\mu = \frac{m_2}{m_1 + m_2} \tag{3}$$

where m_1 and m_2 are the masses of the two primaries. For nondimensionalization, the characteristic quantities include: the distance between the two primaries, l; the combined mass of the primaries, $m_1 + m_2$; and the mean motion of the primaries, n. Thus, in nondimensional units, these quantities are all equal to 1.

When a distant fourth body, P_4, is introduced to the system, a perturbation can be added to the CR3BP to yield an augmented set of equations. Assume that the barycenter of the P_1-P_2-P_4 system moves on a circular path about the P_1-P_2 barycenter, and that P_1 and P_2 continue in their original circular paths; the fourth body acts only to perturb the motion of the spacecraft. This model has been termed the very-restricted four-body problem[9]. The equations of motion become

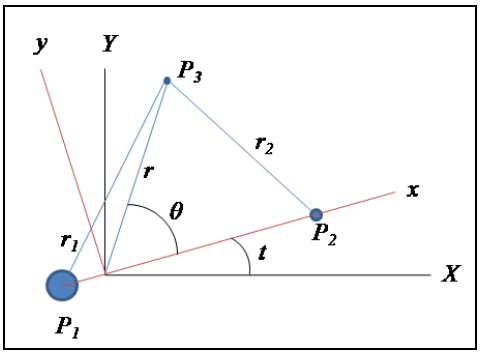

Figure 1. The rotating reference frame in the circular restricted three-body problem, centered at the P_1- P_2 barycenter; inertial axes are denoted by X and Y; x and y rotate with the P_1- P_2 frame.

$$\ddot{x} - 2n\dot{y} - xn^2 = -\frac{(1-\mu)(x+\mu)}{r_1^3} - \frac{\mu(x-(1-\mu))}{r_2^3} - \frac{\mu_4 x_4}{r_4^3} - \frac{\mu_4 x_{cm12-cm124}}{r_{cm12-cm124}^3}$$
$$\ddot{y} + 2n\dot{x} - yn^2 = -\frac{(1-\mu)y}{r_1^3} - \frac{\mu y}{r_2^3} - \frac{\mu_4 y_4}{r_4^3} - \frac{\mu_4 y_{cm12-cm124}}{r_{cm12-cm124}^3} \tag{4}$$
$$\ddot{z} = -\frac{(1-\mu)z}{r_1^3} - \frac{\mu z}{r_2^3} - \frac{\mu_4 z_4}{r_4^3} - \frac{\mu_4 z_{cm12-cm124}}{r_{cm12-cm124}^3}$$

where μ_4 is the nondimensionalized gravitational parameter of the fourth body,

$$\mu_4 = \frac{m_4}{m_1 + m_2} \tag{5}$$

Then, $\bar{r}_4$ is the position vector directed from the fourth body to the spacecraft and $\bar{r}_{cm12-cm124}$ is the position vector from the center of mass of the P_1-P_2 system to the center of mass of the P_1-P_2-P_4 system, shown in Fig. 2. The final term in each of the equations of motion represents an indirect term that compensates for the motion of one barycenter about the other.

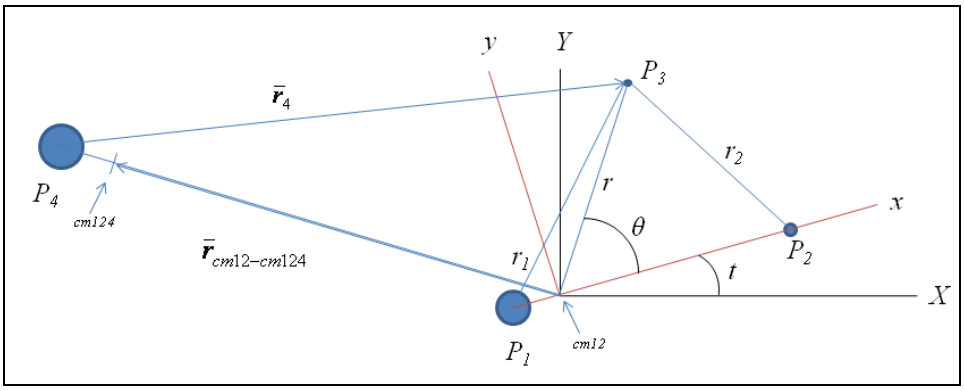

Figure 2. The addition of a distant fourth body to the model in the circular restricted three-body problem. (Not to scale)

B. Energy kick function

Consider a spacecraft moving in a planet-moon system in a relatively large, elliptical, planar orbit about the planet. For the moment, ignore the sun. Measured at apoapsis, assume that the osculating semi-major axis, *a*, and the eccentricity, *e*, of the spacecraft orbit are given. During the next pass, let the spacecraft encounter the moon. Let the gravitational effects of the encounter on the spacecraft orbit from one apoapse passage to the next be modeled as an energy kick applied at periapsis. In the three-body model represented by the CR3BP, the Jacobi Constant does not vary. Thus, this parameter can be employed in estimating the effects of the third-body gravity on the spacecraft orbit. In rotating coordinates, the Jacobi Constant is expressed

$$JC = (x^2 + y^2) + 2\left(\frac{1-\mu}{r_1} + \frac{\mu}{r_2}\right) - \dot{x}^2 - \dot{y}^2 - \dot{z}^2 \tag{6}$$

The Jacobi Constant in the CR3BP can also be written in terms of the inertial coordinates *X* and *Y* and appears in the form

$$JC = 2\left(\frac{1-\mu}{r_1} + \frac{\mu}{r_2}\right) + 2(X\dot{Y} - Y\dot{X}) - \dot{X}^2 - \dot{Y}^2 - \dot{Z}^2 \tag{7}$$

Assuming that $m_2 << m_1$, for a planar orbit, this expression is approximated as follows

$$\begin{aligned} JC \approx & \underbrace{-2\mu\left(\frac{1}{r} - \frac{1}{r_2}\right)}_{} + \underbrace{2\sqrt{a(1-e^2)}}_{} + \underbrace{\frac{1}{a}}_{} \\ = & \quad -2\mu R \qquad\quad -2G \qquad -2K \end{aligned} \tag{8}$$

if it is evaluated in terms of osculating orbital elements. Recall that for small values of μ, or for large values of r and r_2, the Jacobi Constant reduces to the Tisserand Constant,

$$TC = 2\sqrt{a(1-e^2)} + \frac{1}{a} \tag{9}$$

Of course, in the CR3BP, the Tisserand Constant is an approximation and therefore is not, in fact, constant.

In the more complete expression in Eq. (8), the component $K = -\frac{1}{2a}$ can be considered the Keplerian contribution due to the larger primary, and $G = \sqrt{a(1-e^2)}$ is the angular momentum of the spacecraft. The component of the Jacobi Constant contributed by the smaller primary is $\mu R = \mu\left(\frac{1}{r} - \frac{1}{r_2}\right)$, where R can be further approximated as

$$R \approx -\frac{1}{\sqrt{1+r^2-2r\cos\theta}} + \frac{\cos\theta}{r^2} + \frac{1}{r} \tag{10}$$

to first order in μ. The angle between the spacecraft state vector $\bar{r}$ and the rotating x-axis is

$$\theta = \omega + \nu - t = \omega_r + \nu \tag{11}$$

where ω is the spacecraft's argument of periapsis, ν is the true anomaly, t is the angle between the inertial and rotating axes, and ω_r is the argument of periapsis in the rotating coordinate frame, as illustrated in Fig. 3. It is assumed that at the moment of periapsis, the inertial and rotating frames are incident so that $t = \nu = 0$ and $\omega = \omega_r$.

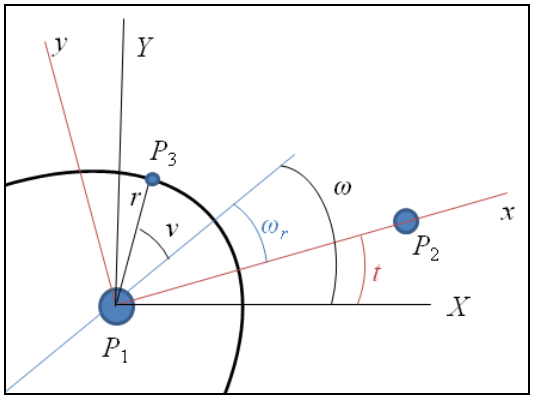

Figure 3. The relationships between the angles ω, ω_r, ν, and t, where X and Y are the inertial axes and x and y rotate with the P_1- P_2 frame.

The component R is considered a perturbing function, and the Lagrange Planetary Equations[14] can be employed to relate R and G such that

$$\frac{dG}{dt} = -\mu\frac{\partial R}{\partial \omega} = -\mu\left(\frac{r}{r_2^3}\sin(\omega+\nu-t) - \frac{1}{r^2}\sin(\omega+\nu-t)\right) \tag{12}$$

Using the Picard method of successive approximations to first order[13],

$$\begin{aligned}\Delta G &= -\mu \int_{-T/2}^{T/2} \frac{\partial R}{\partial \omega} dt \\ &= -\mu \int_{-T/2}^{T/2} \left[\frac{r}{r_2^3} \sin(\omega + \nu - t) - \frac{1}{r^2} \sin(\omega + \nu - t) \right] dt \\ &= -\frac{\mu}{\sqrt{p}} \int_{-\pi}^{\pi} \left[\left(\frac{r}{r_2} \right)^3 \sin(\omega_r + \nu) - \sin(\omega_r + \nu) \right] d\nu \end{aligned} \tag{13}$$

Since the Jacobi Constant does not vary over the trajectory, $\Delta JC = 0$, and from Eq. (8)

$$\mu \Delta R + \Delta G + \Delta K = 0 \tag{14}$$

Over the range of trajectories for the application investigated here, i.e., eccentric orbits in the Saturn-Titan system, the value of $\mu \Delta R$ is four orders of magnitude smaller than ΔG and can be neglected. Therefore, $\Delta K \approx -\Delta G$. Since $K = -\frac{1}{2a}$,

$$\Delta a = \frac{2a^2 \Delta G}{1 - 2a\Delta G} \tag{15}$$

The definite integral in the expression for ΔG is evaluated by quadratures, defining a relationship between Δa and ω_r.

An alternative method for computing Δa is used by Zhou et al.[11] This approach originates with the planar equations of motion in the CR3BP, written in inertial coordinates,

$$\begin{aligned} \ddot{X} &= \frac{(1-\mu)(X_{P1} - X)}{r_1^3} + \frac{\mu(X_{P2} - X)}{r_2^3} \\ \ddot{Y} &= \frac{(1-\mu)(Y_{P1} - Y)}{r_1^3} + \frac{\mu(Y_{P2} - Y)}{r_2^3} \end{aligned} \tag{16}$$

where the *x* and *y* coordinates of the two primaries are

$$\begin{aligned} X_{P1} &= -\mu \cos(t) & X_{P2} &= (1-\mu)\cos(t) \\ Y_{P1} &= -\mu \sin(t) & Y_{P2} &= (1-\mu)\sin(t) \end{aligned} \tag{17}$$

Expanding to first order in μ, the equations of motion become

$$\begin{aligned} \ddot{X} &= \frac{-X}{r^3} + \mu A(X, Y, t) + O(\mu^2) \\ \ddot{Y} &= \frac{-Y}{r^3} + \mu B(X, Y, t) + O(\mu^2) \end{aligned} \tag{18}$$

where

$$A(X,Y,t) = \frac{X - \cos(t)}{r^3} + \frac{3X[X\cos(t) + Y\sin(t)]}{r^5} + \frac{\cos(t) - X}{([X - \cos(t)]^2 + [Y - \sin(t)]^2)^{3/2}}$$

$$B(X,Y,t) = \frac{Y - \cos(t)}{r^3} + \frac{3Y[X\cos(t) + Y\sin(t)]}{r^5} + \frac{\cos(t) - Y}{([X - \cos(t)]^2 + [Y - \sin(t)]^2)^{3/2}} \tag{19}$$

Again, it is assumed that that $t = \nu = 0$ at the moment of periapsis passage. Note that the spacecraft state is a function of the argument of periapsis, ω, which is equal to ω_r when the spacecraft passes through periapsis. Define the Keplerian energy as above, i.e.,

$$K = -\frac{1}{2a} = \frac{\dot{X}^2 + \dot{Y}^2}{2} - \frac{1}{r} \tag{20}$$

and the change in K over time is

$$\frac{dK}{dt} = \mu[\dot{X}(t)A(X(t),Y(t),t) + \dot{Y}(t)B(x(t),Y(t),t)] \tag{21}$$

From one apoapsis passage to the next, the change in K is, therefore,

$$\begin{aligned} \Delta K &= \mu \int_{-T/2}^{T/2} [\dot{X}(t)A(t) + \dot{Y}(t)B(t)]dt \\ &= \frac{\mu r^2}{\sqrt{p}} \int_{-\pi}^{\pi} [\dot{X}(\nu)A(\nu) + \dot{Y}(\nu)B(\nu)]d\nu \end{aligned} \tag{22}$$

The expression in Eq. (18) can, again, be integrated by quadratures such that,

$$\Delta a = \frac{2a^2 \Delta K}{1 - 2a\Delta K} \tag{23}$$

The two methods for calculating Δa yield equivalent results. The second approach is somewhat more straightforward to derive, and may be extended to incorporate additional gravity fields. For only two primaries, however, this second form requires a calculation of the spacecraft state in each integration step and, therefore, requires a longer computation time.

C. Application to the Saturn-Titan system

A potential application of the kick function approach to trajectory and tour design lies in the Saturn-Titan system. A mission such as Cassini employs flybys of Titan to change the orbital parameters and view Saturn and its many satellites from a variety of scientifically interesting perspectives. Since its arrival at Saturn in July 2004, Cassini has completed 45 flybys of Titan. Its prime mission, which lasted through June 30, 2008, incorporated 44 Titan flybys; the 45th flyby occurred on July 31, 2008, the first in its extended mission.[15] Historically, for preliminary design of a tour in a system such as Saturn and its moons, a patched-conic approach is employed.[2-4,15] Such a model assumes that the spacecraft is in a two-body conic orbit about the central body, Saturn. A gravity-assist flyby of Titan is regarded as an instantaneous change in velocity relative to the central body. The period of

the spacecraft orbit can be increased or decreased via orbit pumping, while orbit cranking changes the inclination of the spacecraft orbit relative to the central body. To reach a desired final condition, a series of Titan-to-Titan transfers (i.e., a tour) is employed to control the orbital parameters.[4] Of course, as mission planning proceeds, transition to higher fidelity models is standard and highly successful. However, challenges associated with the patched-conic approach to tour design include determining accurate estimates of flyby parameters such as timing, as well as flyby location and altitude. In addition, in certain regimes patched-conic assumptions cease to hold.[7] If the kick function can be used to characterize the Titan flyby, more accurate estimates of flyby parameters may be available and/or trajectory options that are not exposed in a conic model may become viable possibilities.

Consider a spacecraft in orbit about Saturn (P_1); it is initially located at apoapsis. If the spacecraft encounters Titan (P_2) on its next approach to periapsis, the gravity assist from the Titan flyby will change the spacecraft's orbital parameters, including the osculating semi-major axis. This change in semi-major axis a can be related to the angle between periapsis and the rotating x-axis, ω_r, by the kick function, via the relationships in Eqn. 15 and Eqn. 23. This parameter ω_r can be selected a priori to achieve a desired value of Δa from the Titan flyby. An example of a trajectory with a distant flyby of Titan appears in both inertial and rotating views in Fig. 4.

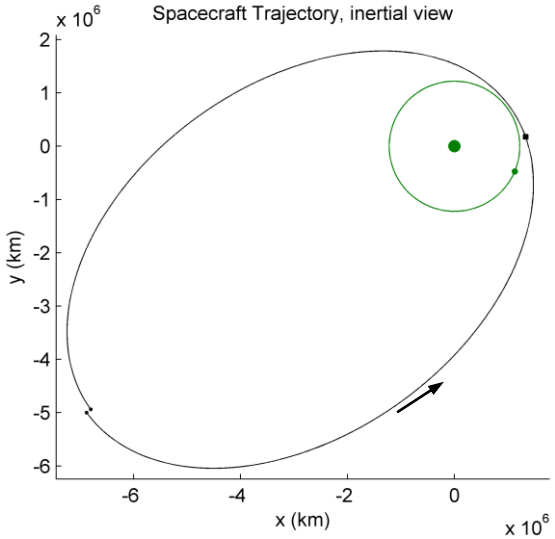

Figure 4a. Inertial view of a trajectory with a = 4, e = 0.74 in the Saturn-Titan system. The locations of Titan and the spacecraft at their closest approach are marked.

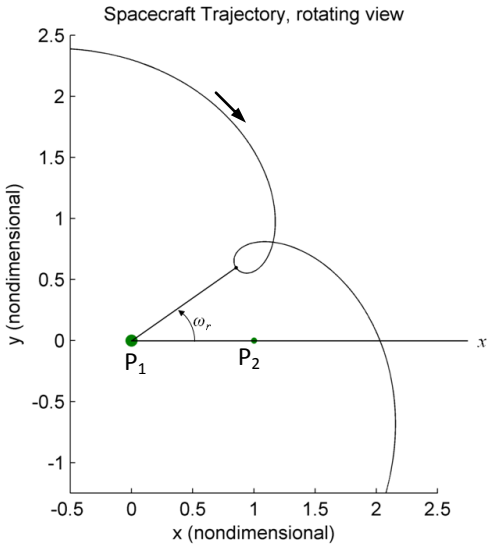

Figure 4b. Rotating view of the same trajectory; the angle between the rotating x-axis and spacecraft periapsis, ω_r, is equal to 0.2π.

Define a variable Q such that

$$Q = \frac{r_{p_{Saturn}}}{R_{Titan}} \tag{24}$$

If the spacecraft periapsis in its Saturn orbit, that is, $r_{p_{Saturn}}$, lies above the orbit of Titan, defined by its circular orbit radius R_{Titan}, then $Q > 1$, as is the case in the trajectory in Fig. 4, and the spacecraft's closest approach to Titan occurs at periapsis. If, however, periapsis dips below the orbit of Titan ($Q < 1$), the spacecraft's closest approach to the moon occurs either before periapsis as an inbound flyby (see Fig. 5) or after periapsis as an outbound encounter (see Fig. 6). Inbound encounters are characterized by positive values of ω_r, outbound flybys by negative values.

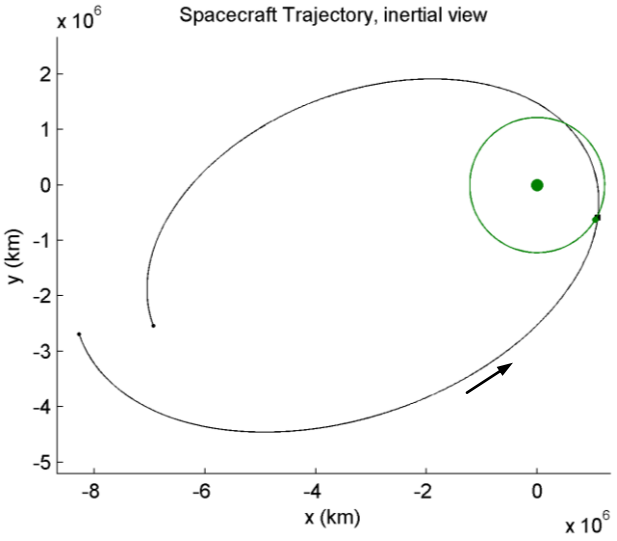

Figure 5a. Inertial view of an inbound flyby with a = 4, e = 0.78 in the Saturn-Titan system. The locations of Titan and the spacecraft at their closest approach are marked.

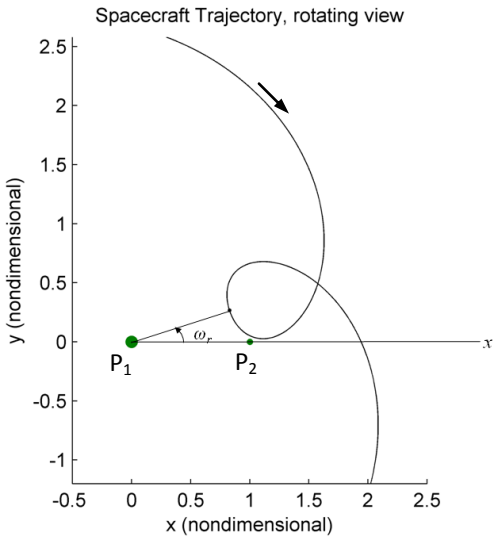

Figure 5b. Rotating view of the same trajectory; the angle between the rotating x-axis and spacecraft periapsis, ω_r, is equal to 0.1π.

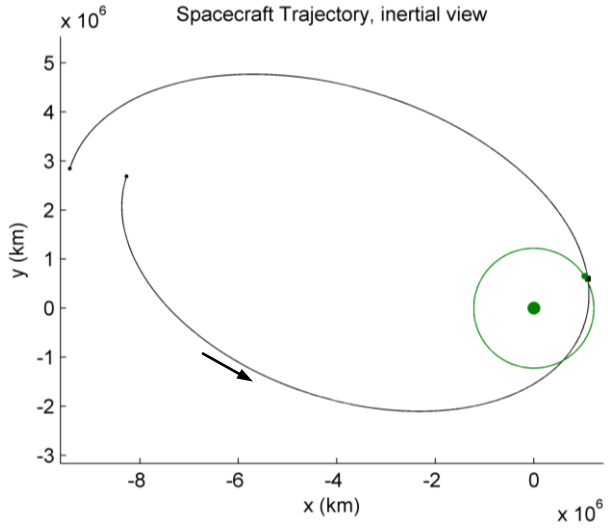

Figure 6a. Inertial view of an outbound flyby with a = 4, e = 0.78 in the Saturn-Titan system. The locations of Titan and the spacecraft at their closest approach are marked.

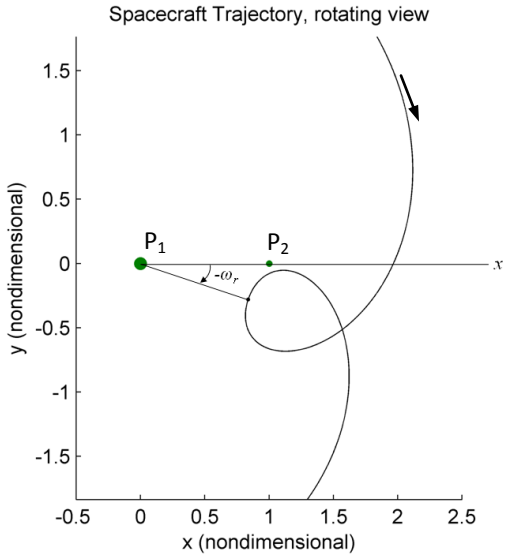

Figure 6b. Rotating view of the same trajectory; the angle between the rotating x-axis and spacecraft periapsis, ω_r, is equal to -0.1π.

For periapse radii either above or below the orbital radius of the second primary, a value of $\omega_r = 0$ results in zero net change in the semi-major axis from apoapsis to apoapsis: targeting a perpendicular crossing of the rotating *x*-axis with a value of semi-major axis that corresponds to a period commensurate with the rotation of the primary system results in a resonant orbit with the second primary and incorporates both gravity fields. Two examples appear in Fig.7.

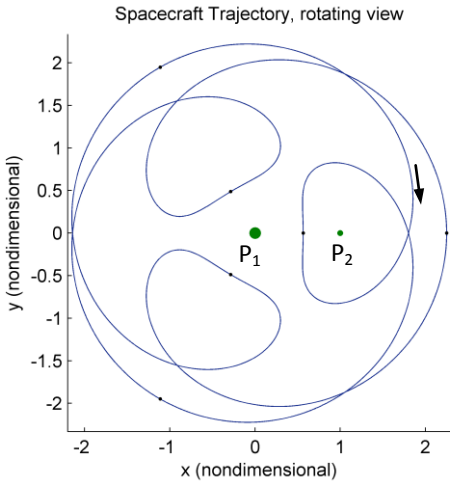

Figure 7a. Rotating view of an orbit with a 3:5 resonance with P_2.

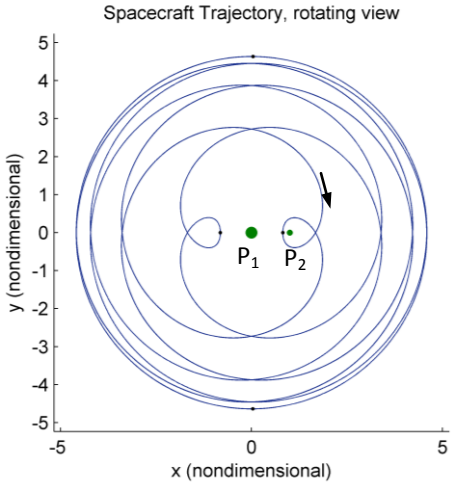

Figure 7b. Rotating view of an orbit with a 2:9 resonance with P_2. Apses are marked with black dots.

The kick function can be employed to approximate the relationship between Δa and ω_r for spacecraft flyby trajectories in many systems; the Saturn-Titan system is used for illustration here. Depending on the trajectory under investigation, the relationship between Δa and ω_r displays certain characteristics. For orbits with periapsis slightly above Titan's orbital radius ($Q > 1$), a single region of values for ω_r centered at $\omega_r = 0$ results in relatively close approaches to Titan and significant changes in semi-major axis. The kick function prediction of the relationship between Δa and ω_r for $Q > 1$ appears in Fig. 8 for initial conditions $a = 4$, e = 0.74. (The value of a is nondimensional; recall that the characteristic length is R_{Titan}). The rotating view of two trajectories, one with a positive value of ω_r and one with a value that is negative, then appears in Fig. 9. When the periapse radius of the spacecraft trajectory dips below the orbit of Titan ($Q < 1$), two regions of ω_r, symmetric about zero, result in close flybys of Titan. For both inbound ($\omega_r > 0$) and outbound ($\omega_r < 0$) encounters, a flyby that leads Titan results in a decreased semi-major axis, while a trailing flyby increases the semi-major axis of the trajectory. Examples of such trajectories appear in Fig. 10. The kick function approximation of the relationship between Δa and ω_r appears in Fig. 11 for both the positive and negative values of the angle ω_r. The analytical expression for Δa (Eqn. (15)) results in an estimate of the actual change in the value of the semi-major axis that a spacecraft will experience due to the gravitational effects of a Titan flyby. The estimate is used to select a target value for the angle ω_r that will yield a desired change in the period of the spacecraft orbit relative to Saturn.

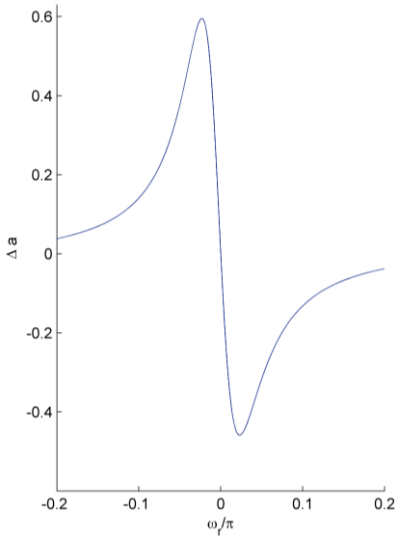

Figure 8. The relationship between Δa and ω_r for $a = 4$, $e = 0.74$, $Q > 1$ in the Saturn-Titan system, as computed from the kick function.

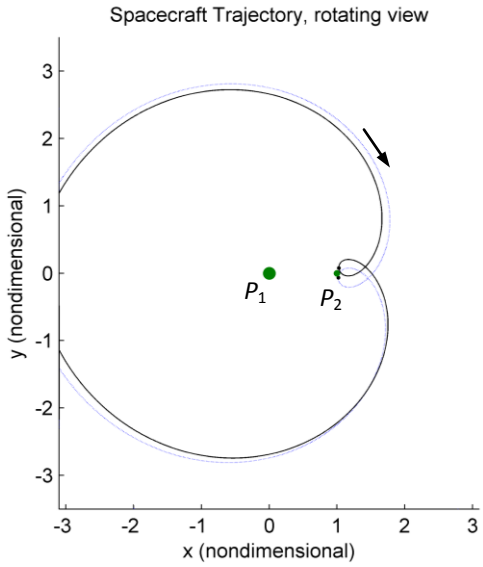

9. Rotating view of two trajectories with $Q > 1$ and values of ω_r mirrored about zero. The periapsis of the orbits with respect to P_1 are marked with black dots.

Figure

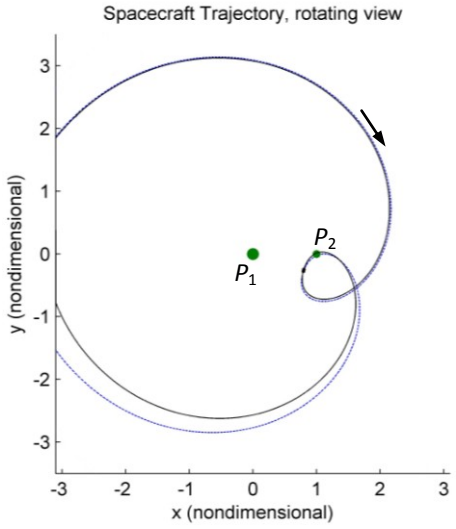

Figure 10a. Rotating view of two trajectories with negative values of ω_r, corresponding to outbound flybys with $Q < 1$.

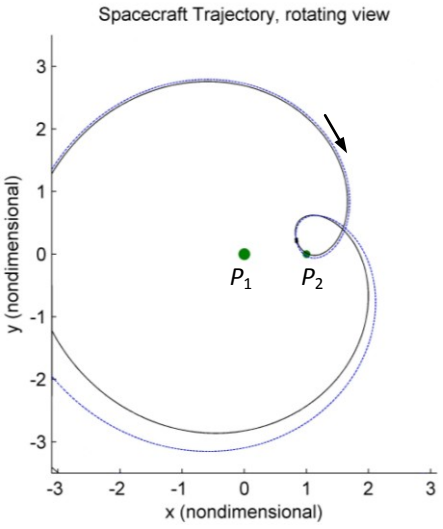

Figure 10b. Similar trajectories with positive values of ω_r: inbound flyby trajectories with $Q < 1$. The periapsis of the orbits with respect to P_1 are marked with black dots.

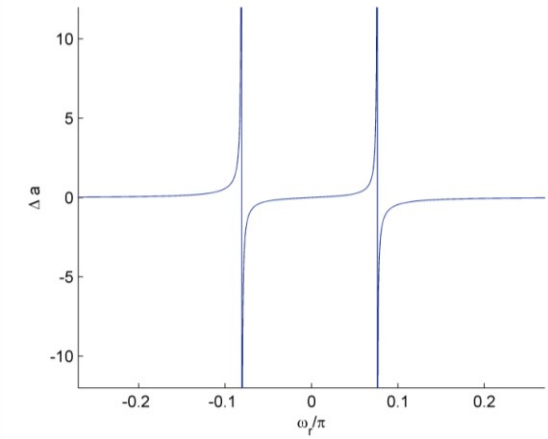

Figure 11. The relationship between Δa and ω_r for a = 4, e = 0.78 and Q < 1 in the Saturn-Titan system, as computed from the kick function for the inbound and outbound flybys.

In Zhou et al.,[11] Pan and Sari,[12] as well as Ross and Scheeres,[13] the kick function is derived for use in a regime with Jacobi Constant slightly greater than 3: nearly circular orbits with $Q > 1$ and relatively distant flybys of the second primary. In such scenarios, the closest approach to the second primary occurs at spacecraft periapsis, in accordance with the modeling of the flyby as an energy kick at spacecraft periapsis. For the orbits investigated in this study, however, the Jacobi Constant is lower, ranging from 2.178 to 2.936, where the values of the Jacobi Constant for the libration points in the Saturn-Titan system range from 2.9998 for L_4 and L_5 to 3.0158 for L_1. The periapse radii of the eccentric orbits dip below Titan's orbital radius, allowing close flybys that do not occur at spacecraft periapsis. In this regime, a correction to the expected Δa must be included to maintain the appropriate level of accuracy required for targeting. Malyshkin and Tremaine,[10] investigating the evolution of highly eccentric orbits with $Q < 1$, use a numerical interpolation scheme. In the current study, the approximate kick function is combined with a numerically calculated correction.

III. Analysis

Designing a Titan flyby to target a specific change in semi-major axis (or orbital period) for a spacecraft orbiting Saturn is first investigated in the Saturn-Titan CR3BP. The accuracy of the relationship between Δa and ω_r as derived from the energy kick function is investigated, an offset is applied to improve the results. Finally, solar gravity is applied to the system and the offset is modified to compensate for the extra force so that the parameter ω_r can adequately characterize the Δa provided by a Titan flyby.

A. Kick function: analytical versus numerical integration

Consider a spacecraft at apoapsis in the Saturn-Titan system, headed towards an outbound Titan encounter. Its trajectory is characterized by a set of osculating orbital elements that change over time due to the influence of Titan. By calculating the change in semi-major axis as the spacecraft orbit evolves from the pre-encounter apoapse position to the post-encounter apoapsis, and by noting the angle of periapsis relative to the rotating x-axis, ω_r, a relationship between Δa and ω_r can be determined. A pair of sample trajectories with initial conditions a = 4 (T = 8 T_t), e = 0.78 appears in Fig. 12. To create two different flybys, the initial line of apsides of the two trajectories differs by 1.8º, or 0.01π. Solely from the numerical propagation, the two paths can be compared. In the figure, the black trajectory is characterized at periapsis by a periapse angle ω_r = -0.0731π, corresponding to a leading flyby of Titan at an altitude of 8,314 km. The semi-major axis at the subsequent apoapsis is a = 2.428, yielding a change in semi-major axis Δa = -1.572. The flyby has caused the new line of apsides to lag the original line of apsides by 13.7º. When ω_r = -0.0829π, demonstrated by the blue trajectory in Fig. 12, the spacecraft trails Titan at a flyby

altitude of 16,815 km, and the semi-major axis is increased to a = 6.923 at the subsequent apoapsis, for a value of Δa = 2.923. The line of apsides has been advanced in this case by 3.03º. Note the high sensitivity of the trajectory to small changes in ω_r. If this process is continued for a range of values of ω_r, a curve relating Δa and ω_r is generated.

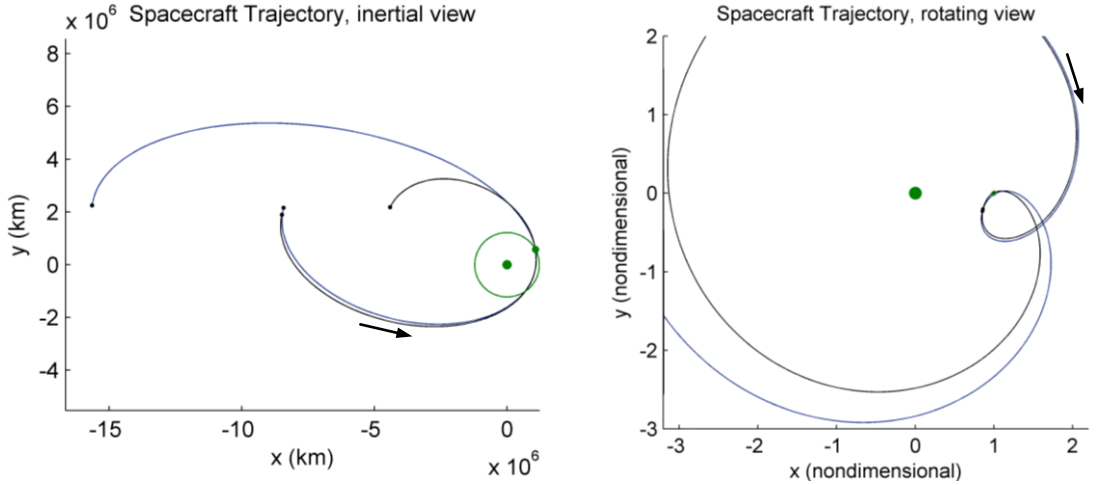

Figure 12. Inertial and rotating views of two trajectories with initial conditions a = 4, e = 0.78.

This relationship between Δa and ω_r can be approximated by the kick function. Because the kick function for $Q < 1$ is symmetric about $\omega_r = 0$, the analysis focuses on negative values of ω_r, or outbound flyby trajectories. The analytical kick function is used to estimate the change in semi-major axis for a range of angles ω_r for each set of initial conditions. First, let the initial semi-major axis correspond to a constant value a = 4 (T = 8 T_t) and modify the initial eccentricity. A modified eccentricity shifts the periapse location as well as the Titan encounter, evidenced by the plots of the kick function in Fig. 13. The value of ω_r that corresponds to the center location becomes more negative with larger initial eccentricity. The general shape of the curves does not change. Now, alter the initial conditions such that eccentricity is fixed at e = 0.78 but three values of semi-major axis are introduced. The results appear in Fig. 14. An increasing value of semi-major axis, a, shifts the center of the kick function curves to increasingly negative values of ω_r, but the shape is consistent.

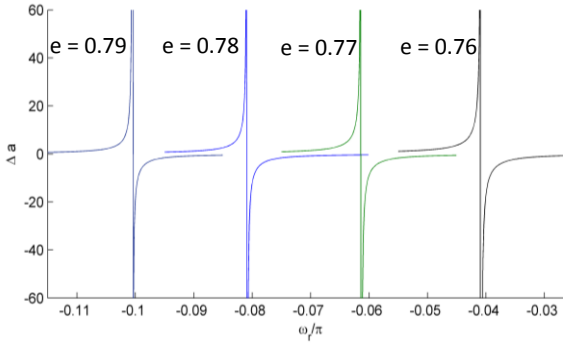

Figure 13. The change in the semi-major axis Δa as a function of the periapse angle ω_r: initial semi-major axis a = 4 (T = 8 T_t); eccentricity e = 0.76-0.79.

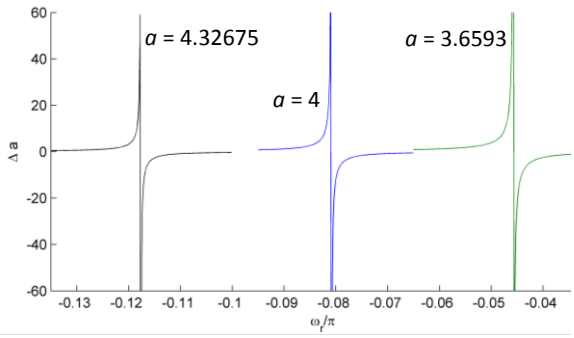

Figure 14. The change in semi-major axis, Δa, as a function of periapse angle, ω_r; initial eccentricity e = 0.78 and semi-major axis: a = 4.32675 (T = 9 T_t); a = 4 (T = 8 T_t); a = 3.6593 (T = 7 T_t).

The advantage to this analytical approach of computing the relationship between Δa and ω_r is the speed with which the curves can be generated: for a given set of initial conditions, an estimate of the angle ω_r required to achieve a desired Δa can be quickly determined. However, these relationships between Δa and ω_r contain approximations. By numerically integrating a set of trajectories with a range of values of ω_r from apoapsis to apoapsis in the CR3B model, the actual relationship between Δa and ω_r can be calculated and compared to the analytical approximations. For example, for initial conditions at apoapsis $a = 4$, $e = 0.78$, the analytical and numerically integrated curves of Δa versus ω_r appear in Fig. 15. Note that the general shape of the predicted analytical results and the numerically integrated curves is the same. The 'center' of the numerical curve has shifted, resulting in an offset. This offset represents the assumptions and approximations inherent in the analytical kick function. Recall that in the derivation of the kick function, the assumption is made that at the moment of periapsis, the rotating and inertial axes are coincident such that $\omega = \omega_r$ and $t = 0$. However, in a mission design scenario, particularly one incorporating multiple flybys, it cannot be guaranteed that this will be the case. This difference between ω and ω_r in the numerically integrated trajectories at the moment of periapsis accounts for the majority of the offset. (Note that in the curve representing the numerically integrated trajectories, a flat region represents a set of trajectories associated with extremely close flybys: within the surface of Titan. These trajectories have been removed from the numerical curve.)

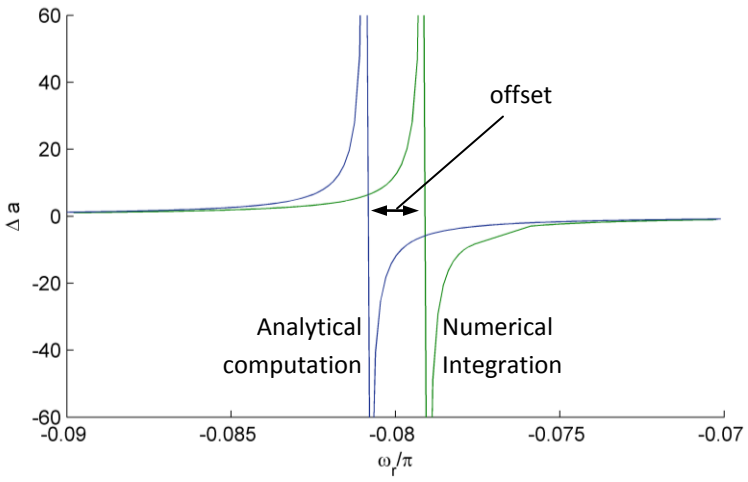

Figure 15. Analytical and numerical relationships between Δa and ω_r for $e = 0.78$ and $a = 4$ at initial apoapsis.

B. Targeting a specific periapsis angle

The offset between the curves in Fig. 15 relates the analytical kick function to the numerically integrated relationship between Δa and ω_r for a series of trajectories with a certain set of initial conditions in terms of the osculating values of a and e and the orientation between the rotating and inertial axes. However, for trajectory design applications, it is also advantageous to note how the numerical value corresponding to the offset changes if a specific value of ω_r is targeted from apoapsis. In this scenario, each trajectory is initially at apoapsis with a given value of a and e. A ΔV between 0-35 m/s is applied to the initial state to target a desired angle of periapsis with respect to the rotating x-axis, ω_r. A very significant observation is that the ΔV changes the osculating values of a and e at the initial state. For example, for a trajectory with initial values such that $a = 4$, $e = 0.78$ at apoapsis, a ΔV of 26 m/s can be applied to target a value of $\omega_r = -0.1\pi$. This ΔV changes the initial semi-major axis and eccentricity and the new adjusted (targeted) trajectory possesses an osculating semi-major axis value $a = 3.9782$ and eccentricity $e = 0.790$. The targeted and untargeted trajectories appear in Fig. 16 in the inertial and rotating views. The blue trajectory arc is the original path; the ΔV is reflected in the black trajectory. By adding the ΔV at apoapsis and changing the initial a and e, the relationship between Δa and ω_r has been shifted.

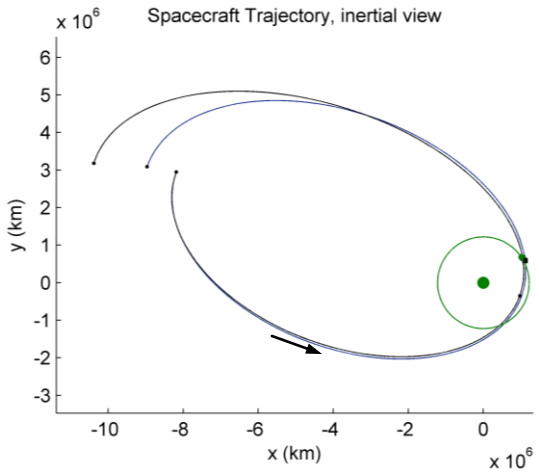

Figure 16a. Inertial view of a pair of trajectories. The original trajectory appears in blue; initial conditions are a = 4 e = 0.78. The black orbit is targeted to reach ω_r = -0.11π; the resulting initial conditions are a = 3.9782 and e = 0.790.

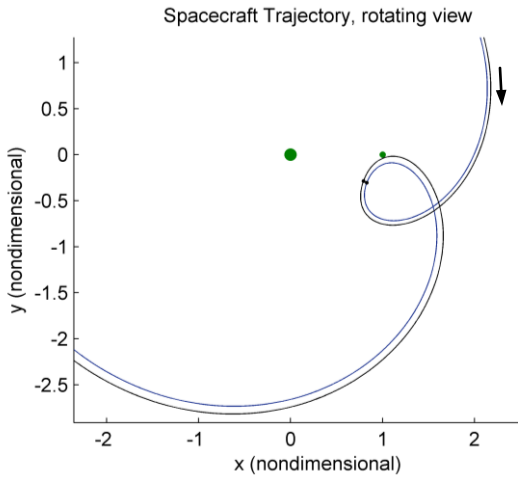

Figure 16b. Rotating view of the same two trajectories.

If the Δa due to the Titan flyby is plotted against the targeted value of ω_r, the resulting curve can again be compared to the analytical kick function. The analytical kick function is computed both with the original values a = 4 and e = 0.78, as well as with new values a = 3.9782 and e = 0.790 that correspond to the osculating elements at apoapsis after the targeting ΔV has been applied for ω_r = -0.1π. Note that each targeted value of ω_r requires a different ΔV, which yields a different set of elements a and e and therefore a different associated analytical curve. The targeted numerical curve and the two analytical curves relating Δa and ω_r appear in Fig. 17. The offset between the targeted numerical integration and the analytical computation now reflects a combination of the difference between ω and ω_r at periapsis passage, the changing values of initial a and e due to the applied ΔV, and other assumptions involved in the kick function expression.

From Fig. 17, it is clear that if the analytical function computed using the original osculating elements a and e is used to select a value of ω_r for targeting with the goal of achieving a specific Δa, the resulting numerically integrated trajectory will not reach the desired semi-major axis. As an example, consider a trajectory with initial a = 4, e = 0.78. Assume that a particular change in semi-major axis is required; for example, Δa = 2. For these initial conditions, the analytical kick function recommends targeting a value of ω_r = -0.0863π to achieve Δa = 2. However, when this value of ω_r is targeted, the actual change in semi-major axis from the pre-flyby apoapsis to the post-flyby apoapsis is Δa = -0.447. Fortunately, the offset can be subtracted from the estimate of ω_r to improve the outcome significantly. In this example, the angle offset is 0.01976π. When it is applied to the analytical kick function, the new recommended angle of

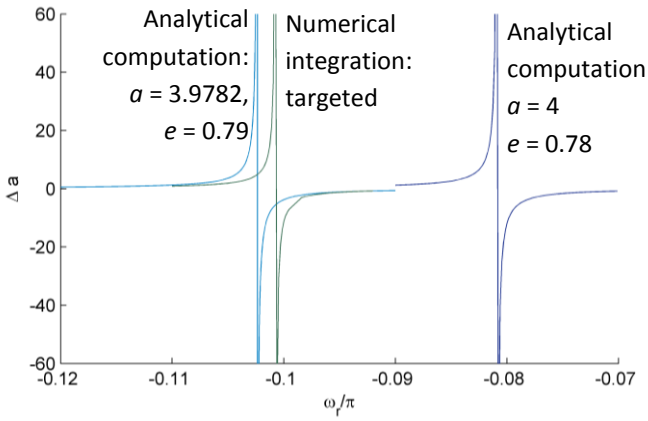

Figure 17. The change in the semi-major axis Δa as a function of the periapse angle ω_r, as calculated by the analytical kick function and by numerical integration of a set of trajectories, with and without targeting.

periapsis is ω_r = -0.10606π, which yields Δa = 1.516: much closer to the desired change in semi-major axis. (At this time, this process does not update the semi-major axis and eccentricity values in the iteration process. Such a step is possible and will likely speed the convergence.)

For simplicity, assume that the original values of *a* and *e* are retained throughout the iterations. The offset is calculated for various sets of initial conditions. When the offset is plotted against the initial period, a pattern emerges structured in terms of initial eccentricity. Seven curves, each representing a different value of initial eccentricity, appear in Fig. 18. Each curve consists of a 4th-order polynomial fit of offset as a function of the original osculating period.

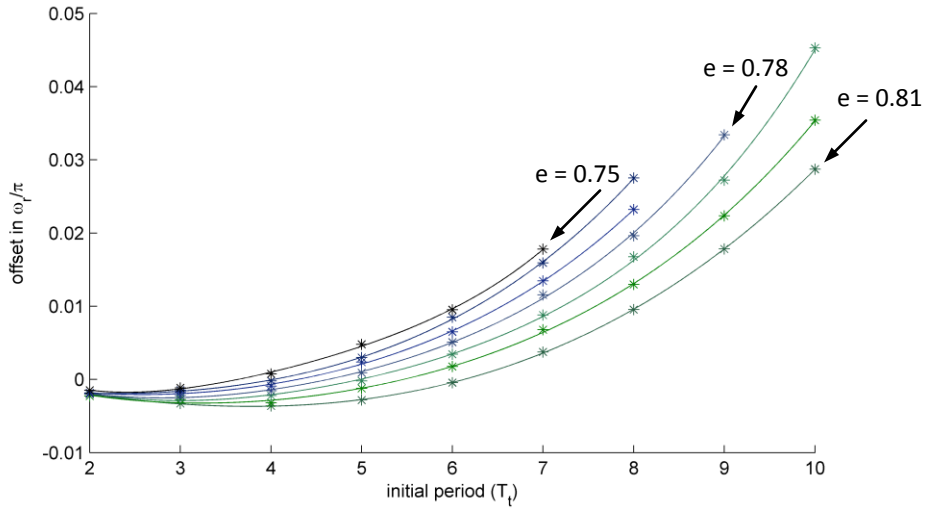

Figure 18. Offset in zero-crossing as a function of initial period for values of semi-major axis between a = 1.5874 (T = 2 T_t) = and a = 4.64159 (T = 10 T_t) and eccentricity e = 0.75 to e = 0.81.

When combined with the analytical estimate, as in the previous example, an improved target value of ω_r is obtained. To evaluate the utility of the offset for several additional cases, the analytical kick function is computed for a = 4 (T = 8 T_t), e = 0.79. The resulting relationship between Δa and ω_r is used to select target values for ω_r to achieve a set of specific orbital periods at the subsequent apoapse passage, ranging from 2 T_t to 18 T_t. The trajectory is then numerically integrated, and the actual period at the post-flyby apoapsis is calculated. Similarly, the trajectory is numerically integrated targeting the improved value of ω_r obtained by subtracting the offset from the original kick function estimate. (Note that for positive values of ω_r, the offset is added to the estimate.) The desired orbital periods and the actual periods with and without the offset appear in Table 2.

Table 2. Osculating periods at post-flyby apoapsis after targeting values of ω_r, with and without the offset, compared to desired orbital periods; initial elements a = 4, period = 8 T_t, e = 0.79; a and e are not updated during iterations.

Initial osculating elements at apoapsis (before application of targeting ΔV): a = 4, period = 8 T_t, e = 0.79		
target period (Titan revs)	final period: no offset applied to target ω_r	final period: with offset applied to target ω_r
18	6.6376	15.1132
17	6.6001	14.4465
16	6.5510	13.7750
15	6.4811	13.0784
14	6.3773	12.3759
13	6.2121	11.6711
12	5.8919	10.9521
11	5.0423	10.2208

Initial osculating elements at apoapsis (before application of targeting ΔV): a = 4, period = 8 T_t, e = 0.79		
target period (Titan revs)	final period: no offset applied to target ω_r	final period: with offset applied to target ω_r
10	escape	9.4791
7	7.5656	7.1737
6	7.3972	6.3941
5	7.2968	5.5918
4	7.2295	4.7685
3	7.1796	3.9048
2	7.1411	3.0119

From the values in Table 2, it is apparent that by including the offset in the targeted value of ω_r, the orbital period after the Titan flyby becomes significantly closer to the desired period. However, there still is not an exact match. The differences between the desired and actual orbital periods at the post-flyby apoapse passage with the offset included in the targeted values of ω_r appear in Fig. 19 for the example. Note the linearity of the curve. Table 2 and Fig. 19 are obtained with the simplest iteration scheme possible. From the information in Table 2, it is straightforward to incorporate one more step to render the target periods. When the actual value of ω_r required to reach a specific change in semi-major axis or period is computed in the numerically integrated CR3BP, an additional offset to the estimated value is determined. For the example, with a = 4 (T = 8 T_t), e = 0.79, the additional offset, which compensates for the approximations in the kick function, appears in Fig. 20.

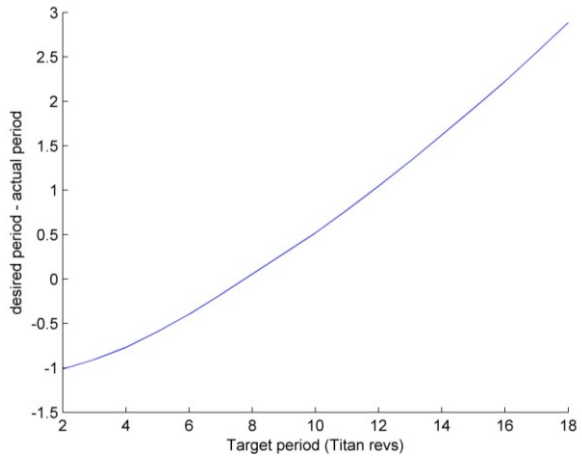

Figure 19. Desired orbital period minus actual period for a variety of targets. Initial conditions a = 4 (T = 8 T_t), e = 0.79, offset included.

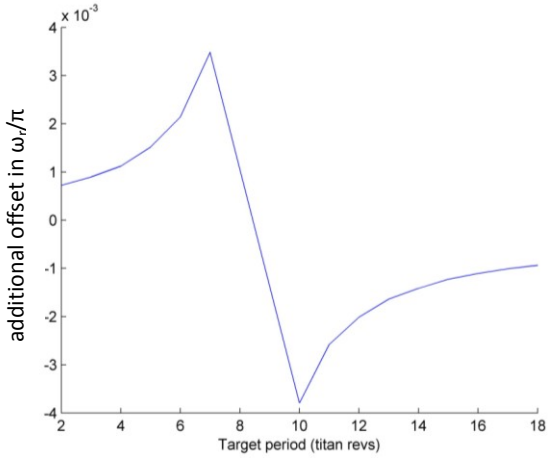

Figure 20. Additional offset required to reach desired period.

These data demonstrate that the offset required to meet a desired change in semi-major axis from a targeted Titan flyby can be accommodated with a relatively simple, straightforward strategy. More sophisticated algorithms can be developed. Prior to further examination, however, it is useful to consider the addition of a 4th gravitational field that will perturb the motion.

C. Effects of Solar Gravity by Quadrant

While the sun is a distant body relative to a spacecraft moving in the Saturn-Titan system, its impact as a perturbing force can be significant on large orbits. The direction of the perturbing acceleration due to solar gravity on any spacecraft in a planetary orbit depends on the orientation of the spacecraft's orbit relative to the sun and planet, in this case, Saturn.[16,17] Thus, to investigate this force and exploit it for trajectory design, observations in terms of a coordinate frame that rotates with the planet (Saturn) about the sun are insightful. A Saturn-centered rotating frame is defined to facilitate the analysis. Let the ξ,η plane represent Saturn's orbital plane. The ξ-axis is fixed along the sun-Saturn line and the η-axis is perpendicular to the ξ-axis, defined as positive in the general direction of Saturn's orbital velocity. Four quadrants centered at Saturn are defined in the rotating frame and appear in Fig. 21. The quadrants are defined in a counterclockwise fashion, with quadrant I on the far side of Saturn and leading Saturn in its orbit. When the spacecraft orbit is viewed in this rotating frame, its orientation is defined by the quadrant that contains the orbit apoapsis. In the current work, the angle of orientation ϕ within each quadrant is defined as the angle from the sun-Saturn line. The positive sense of the angle in each quadrant is defined in Fig. 21.

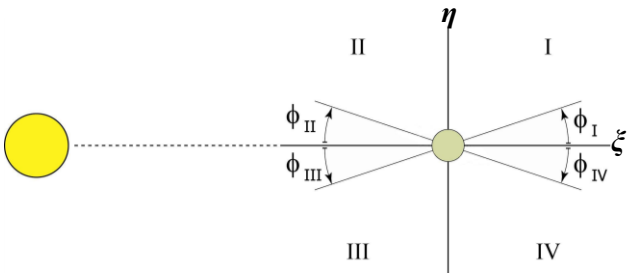

Figure 21. Quadrants and orientation angles as defined in the rotating frame.

Consider a spacecraft in orbit about Saturn. In all quadrants, the effects on the spacecraft are greatest near apoapsis. In quadrants I and III, the direction of the perturbing tidal acceleration generally opposes the direction of motion in a prograde orbit. In quadrants II and IV, on the other hand, the net perturbing acceleration at apoapsis is in the same direction as the motion along a prograde orbit. As a result, the tidal effects are similar in diagonal quadrants. For example, solar gravity perturbations tend to circularize prograde orbits lying in quadrants II and IV and to elongate prograde orbits with an apoapsis in either quadrant I or quadrant III.

For sufficiently large orbits, solar gravity can significantly change the orbital elements. Consider a prograde orbit large enough to be impacted significantly by the Sun but sufficiently small such that the solar gravitational perturbations do not cause the orbit to become retrograde or to escape. A comparison between the characteristics of the spacecraft orbit from one apoapsis to the next demonstrates the solar influence. If the apoapsis originally lies in quadrant I or III, solar gravity will raise the apoapse radius and increase eccentricity at the subsequent apoapsis. Alternatively, if apoapsis lies in quadrant II or IV, solar gravity will lower the apoapse radius and decrease eccentricity. These results are summarized in Table 3.

For a given orbit at a specified orientation angle, the solar gravitational perturbations have maximum effect when the orbit lies in the ecliptic plane. Note that Saturn's equatorial plane is inclined at about 26.7º with respect to the ecliptic. Also, within each quadrant, solar perturbations in a, r_p, r_a and e are at a maximum when apoapsis lies at approximately 45º from the sun-Saturn line (see Fig. 20), although the precise angle varies as the period of the orbit changes.[17] For a 127.6-day orbit, the changes in osculating orbital elements

Table 3. Effects of solar gravitational perturbations on osculating orbital elements; measured from apoapsis to apoapsis.

	Quadrants I and III	Quadrants II and IV
Semi-major axis	increases	decreases
Periapse radius	decreases	increases
Apoapse radius	increases	decreases
Eccentricity	increases	decreases

between subsequent apoapsis passages appear in Fig. 22a. The effects grow as the size of the orbit increases. For an orbit with a period of 318.9 days, the changes in osculating elements between apoapsis passages appear in Fig. 22b. For this investigation it is assumed that the problem is planar. This corresponds to a situation in which the line of nodes of Saturn's orbit about the sun is aligned with that of Titan's orbit about Saturn for the maximum gravitational perturbation from the sun.

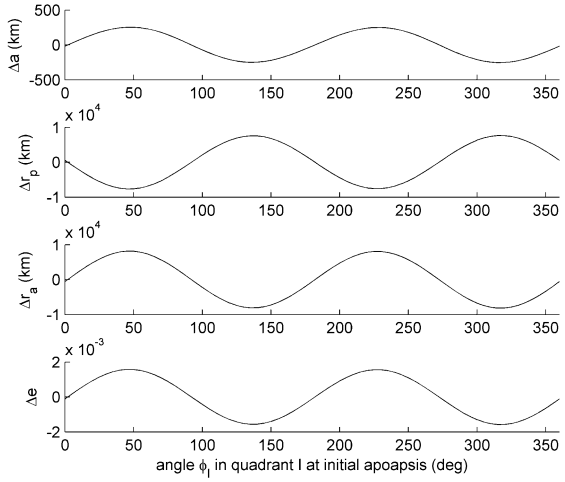

Figure 22a. Changes in orbital elements from one apoapsis to the next as a function of quadrant angle ϕ_I: 127.6-day orbit.

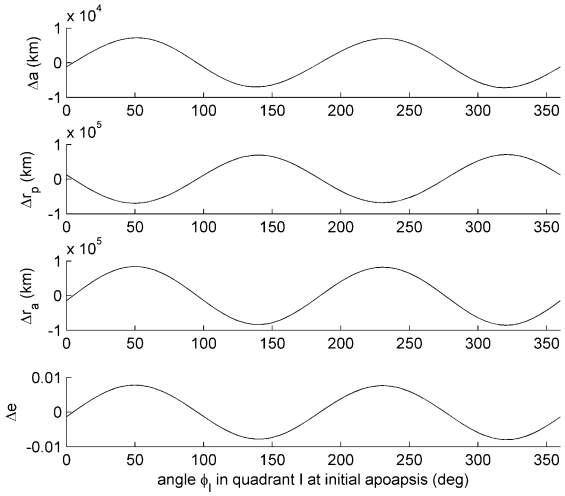

Figure 22b. Same, for a 318.9-day orbit

D. Four-body kick function

When the solar gravitational acceleration is added to the CR3BP equations of motion, the numerically integrated curve relating Δa to ω_r is shifted. The magnitude and direction of the shift depend on the orientation of the spacecraft orbit in the sun-Saturn rotating frame as well as the orbit size and inclination. Consider a spacecraft orbit with initial conditions $a = 4$, $e = 0.78$, aligned such that apoapsis lies in quadrant II in the Sun-Saturn rotating frame. The period of the orbit is 8 T_t = 127.6 days; the effects of solar gravity are not insignificant and are apparent in a plot of the trajectory. In Fig. 23, the unperturbed trajectory (no solar influence) appears in black. With the sun's gravitational perturbation included, the effects on the orbit at periapsis are reflected in the green curve. The periapse radius is increased and the periapse angle ω_r is decreased (i.e., becomes more negative). When the orbit is oriented in quadrant III, the periapse angle is increased and the periapse radius is lowered, as demonstrated by the blue trajectory.

When the trajectory is propagated through to the second apoapsis passage, the change in semi-major axis, Δa, can be computed. When a series of trajectories with varying values of ω_r is propagated, the relationship between Δa and ω_r emerges as before. These curves for three examples appear in Fig. 24. Clearly, compared to the trajectory in black that is not influenced by the sun, the function shifts to the right when apoapsis lies in quadrant II (green curve) and to the left when apoapsis is in quadrant III (blue curve). The same analysis can be completed for a

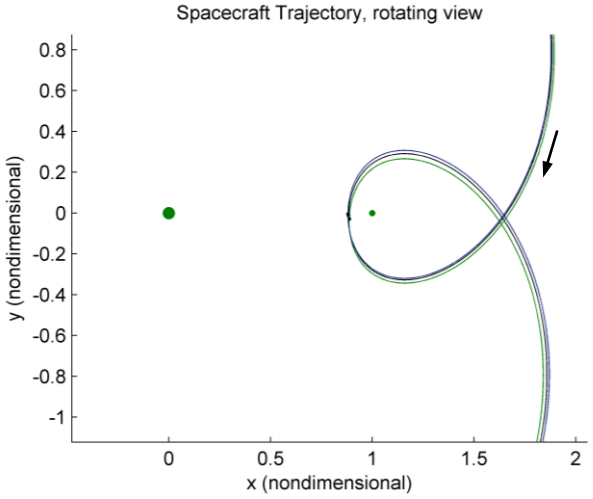

Figure 23. Trajectory with no solar influence plotted in black; Trajectory oriented in solar quadrant II in green; in solar quadrant III in blue.

trajectory that initially possesses a large semi-major axis value and appears in Fig. 25. As expected, the shift in the kick function increases with the increase in effects from the solar perturbation for a larger orbit. This shift appears predictable and can be incorporated in an estimate of the kick functions. It is noted that the shift will be dependent, not only on the solar quadrant, but also on the on the exact orientation within the quadrant. Figures 24 and 25 include the maximum possible impact.

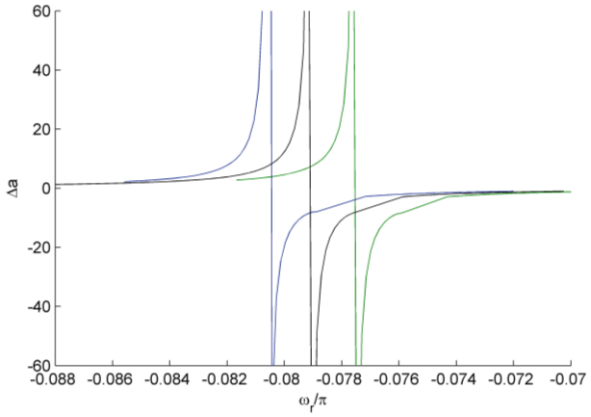

Figure 24. The change in the semi-major axis Δa as a function of the periapse angle ω_r for initial osculating elements $a = 4$, $T = 8T_t$, $e = 0.78$. Trajectory in black includes no solar influence; trajectory in quadrant III in blue; trajectory in quadrant II in green.

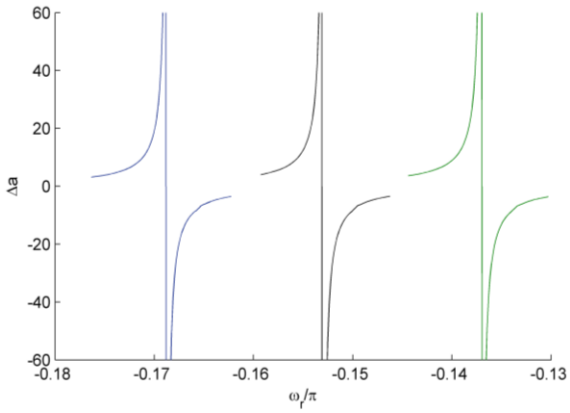

Figure 25. The change in the semi-major axis Δa as a function of the periapse angle ω_r for initial osculating elements $a = 7.368$, $T = 20T_t$, $e = 0.78$. Trajectory in black includes no solar influence; trajectory in quadrant III in blue; trajectory in quadrant II in green.

E. Targeting a specific periapse angle in the 4-body model

As in the case without the sun, it is desirable to maintain the ability to target to a moon periapsis flyby angle when the sun is included in the gravity model. Targeting can still be accomplished even though the sun exerts a large influence and, in this example, the simplest targeting strategy is employed. If the same procedure is applied, i.e., the initial osculating states elements values for a and e are not updated during the iteration process to compute modified target values of the angle ω_r, the scheme can still successfully yield the specified change in the semi-major axis computed at apoapsis. Such a result is plotted in Fig. 26. Depending on the solar quadrant as well as choice of initial conditions, the ΔV required to target a specific value of ω_r can be as little as a few m/s or on the order of 100 m/s.

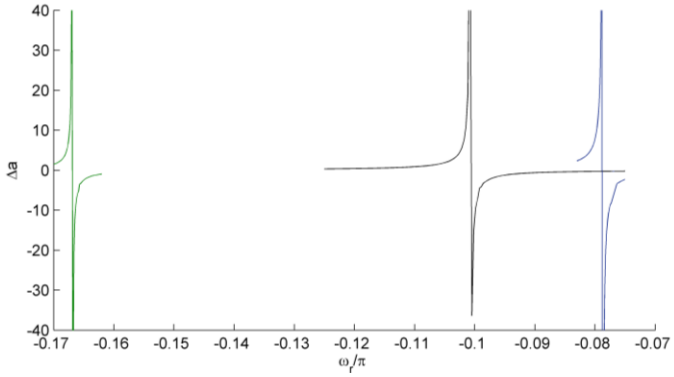

Figure 26. The change in the semi-major axis Δa as a function of the targeted periapse angle ω_r for $a = 4$, $T = 8T_t$, $e = 0.78$. Trajectory in quadrant III in blue; trajectory in quadrant II in green; unperturbed trajectory in black.

IV. Concluding Remarks

The energy kick function has been explored as an approach to estimate the value of the periapsis angle ω_r, as a design variable for a flyby of a moon, to change the semi-major axis of an orbit in the presence of two or three gravity fields. Even though the focus of this application is close flybys, such that $Q < 1$, the kick function can be successfully exploited to yield the desired relationships. Incorporating an offset compensates for the approximations and assumptions in the analytical kick function and appears to be predictable.

This work represents a first step in the process of developing a design strategy that incorporates multiple gravity fields. These principles may be used at Saturn with its single large moon, but it also may be employed in the Jupiter system, where multiple satellites are available to provide significant gravity assists. A next step is to remove the delta velocity by adjusting the timing and position of the spacecraft apoapses to yield the desired angles ω_r, and to extend the work to a series of flybys. A further adjustment to the analytical kick function to include the gravity of additional bodies is ongoing.

Acknowledgments

The authors would like to thank the Clare Booth Luce Program as well as Purdue University. Currently, D. Davis is supported through a Graduate Assistance in Areas of National Need (GAANN) Fellowship.

References

[1] Diehl, R., D. Kaplan, and P. Penzo, "Satellite Tour Design for the Galileo Mission," Paper No. AIAA-83-0101, AIAA 21st Aerospace Sciences Meeting, Reno, Nevada, January 10-13, 1983.

[2] Wolf, A., "Touring the Saturnian System," *Space Science Reviews*, Vol. 104, 2002, pp. 101-128.

[3] Wolf, A. and J. Smith. "Design of the Cassini Tour Trajectory in the Saturnian System," *Control Engineering Practice*, Vol. 3, No. 11, Oct. 1995, pp. 1611-1619.

[4] Yam, C., D. Davis, J. Longuski, and K. Howell, "Saturn Impact Trajectories for Cassini End-of-Life", Paper No. AAS 07-257, AAS/AIAA Astrodynamics Specialist Conference, Mackinac Island, Michigan, August 19-23, 2007.

[5] Heaton, A., N. Strange, and J. Longuski, "Automated Design of the Europa Orbiter Tour," *Journal of Spacecraft and Rocket*s, Vol. 39, No. 1, January-February 2002.

[6] Ludwinski, J., M. Guman, J. Johannesen, R. Mitchell and R. Staehle [1998], The Europa Orbiter Mission Design, Paper No. 98-4.2.02, presented at the 49th International Astronautical Congress, Melbourne, Australia, September 28 - October 2, 1998.

[7] Sweetser, T., R. Maddock, J. Johannesen, J. Bell, P. Penzo, A. Wolf, S. Williams, S. Matousek, and S. Weinstein, Trajectory Design for a Europa Orbiter Mission: A Plethora of Astrodynamic Challenges, Paper No. AAS 97-174, AAS/AIAA Space Flight Mechanics Meeting, Huntsville, Alabama, February 1997.

[8] Ross, S., W. Koon, M. Lo, and J. Marsden, "Design of a Multi-Moon Orbiter," Paper No. AAS 03-143, 13th AAS/AIAA Space Flight Mechanics Meeting, Ponce, Puerto Rico, February 9-13, 2003.

[9] Howell, K. and J. Guzmán, "Spacecraft Trajectory Design in the Context of a Coherent Restricted Four-Body Problem with Application to the MAP Mission," Paper No. IAF-00-A.5.06, 51st International Astronautical Congress, Rio de Janeiro, Brazil, October 2-6, 2000.

[10] Malyshkin, L. and S. Tremaine, "The Keplerian Map for the Planar Restricted Three-Body Problem as a Model of Comet Evolution," *Icarus*, Vol. 141, 1999, pp. 341-353.

[11] Zhou, J., Y. Sun, J. Zheng, and M. Valtonen, "The transfer of comets from near-parabolic to short-period orbits: map approach," *Astronomy and Astrophysics*, Vol. 364, 2000, pp. 887-893.

[12] Pan, M. and R. Sari, "A Generealization of the Lagrangian Points: Studies of Resonance for Highly Eccentric Orbits," *The Astronomical Journal*, Vol. 128, September 2004, pp. 1418-1429.

[13] Ross, S. and D. Scheeres, "Multiple Gravity Assists, Capture, and Escape in the Restricted Three-Body Problem," *SIAM Journal of Applied Dynamical Systems*, Vol. 6, No. 3, 2007, pp. 576-596.

[14] Taff, L. *Celestial Mechanics*. John Wiley & Sons Inc., New York, 1985.

[15] Cassini-Huygens Home [http://saturn.jpl.nasa.gov/home/index.cfm, Accessed 8/7/08].

[16] Yamakawa, H., J. Kawaguchi, N. Ishil, and H. Matsuo, "On Earth-Moon Transfer Trajectory with Gravitational Capture," Paper No. AAS 93-633, AAS/AIAA Astrodynamics Specialist Conference, Victoria, Canada, August 16-19, 1993.

[17] Davis, D., C. Patterson, and K. Howell, "Solar Gravity Perturbations to Facilitate Long-term Orbits: Application to Cassini," Paper No. AAS 07-275, AAS/AIAA Astrodynamics Specialist Conference, Mackinac Island, Michigan, August 19-23, 2007.